Dalton Transactions

COMMUNICATION

Cite this: *Dalton Trans.*, 2016, **45**, 14019

Received 28th April 2016, Accepted 4th August 2016

DOI: 10.1039/c6dt01667g

www.rsc.org/dalton

Nanoparticles of lanthanide oxysulfate/oxysulfide for improved oxygen storage/release†

Wuyuan Zhang, Isabel. W. C. E. Arends and Kristina Djanashvili*

Lanthanide oxysulfates have the ability to store and release large volumes of oxygen under oxidizing/reducing conditions, rendering them interesting as automotive catalysts. Herein we demonstrate a remarkable improvement of both processes by utilization of nanoparticles compared to the bulk materials. A further improvement of the catalytic activity was achieved by cost-effective doping with 1.9 wt% of Ni.

Materials with a capacity for oxygen storage and release are important oxygen carriers (OCs) and are therefore of great interest for application in automotive catalytic combustion. Under oxidative conditions, metal oxides are formed, which then in turn can be reduced by fuel components, such as CO, hydrocarbons, and NO_x. In this process, OCs undergo a reversible and quantifiable redox reaction with oxygen in the gas phase or at the gas–solid interphase, and are therefore useful for regulation of the oxygen concentration under oxygen lean conditions.[1–3] Commonly, transition metal oxides on various supports, *e.g.* dendrimers, TiO_2, Al_2O_3, zeolites, SiO_2, *etc.* have been studied for this purpose.[4] CeO_2 is an attractive material in this respect because of the reversible and fast redox reactions between Ce^{4+} and Ce^{3+} at relatively mild temperatures (<400 °C). Much effort has been put into control of the surface properties of this material to minimize deactivation due to sintering at operation temperatures. Strategies have been developed to increase surface area and/or to create more distorted structures, such as dispersion of ceria into porous carriers,[5] creation of defects,[6,7] chemical doping,[8–10] and reduction of the particle size.[11–14] The latter objective is among the most important factors that are influencing the oxygen storage capacity of OCs.

However, the maximum capacity of oxygen storage per mole of CeO_2 is limited to 0.25 mole of O_2 and its stability is not sufficient under operating conditions.[15] Another disadvantage of metal oxides is their susceptibility to sulfur poisoning when using common carbon fuels.[16,17] $CaSO_4$ has been extensively studied due to its sulfur tolerance along with the capacity to store up to 2 mol of O_2 per mol of sulfate.[18,19] However, high reduction rates can be only achieved above 1000 °C, accompanied with some undesired release of SO_2.[20]

In 2004, Machida *et al.* reported a promising alternative by using lanthanide oxysulfates ($Ln_2O_2SO_4$) with much larger capacities of oxygen storage (2 mole of O_2 per mole of S).[21] The mechanism of the oxygen storage, in this case, does not involve the metal ions, but is based on the reversible redox of sulfur from +6 (SO_4^{2-}) to −2 in sulfide (S^{2-}),[1] as shown in the following reactions:

$$Ln_2O_2SO_4 + 4H_2 \rightarrow Ln_2O_2S + 4H_2O \quad (1)$$

$$Ln_2O_2S + 2O_2 \rightarrow Ln_2O_2SO_4 \quad (2)$$

Another advantage of $Ln_2O_2SO_4$ is the very large stability and catalytic activity up to very high temperatures (>1000 °C), without the loss of sulfur. Moreover, a wide range of lanthanides can be applied for this purpose.[1,22] On the other hand, the practical application is limited due to the still high temperatures (>700 °C) required. Impregnation of $Ln_2O_2SO_4$ materials with noble metals (Pt or Pd) resulted in significant reduction of the operative temperatures by 100–200 °C for both oxygen release and storage processes due to the activation of hydrogen and oxygen spillover.[21] The reaction rates could also be enhanced by increasing the surface of the $Ln_2O_2SO_4$ materials by using layered Ln-dodecyl sulfate mesophases as precursors during its preparation.[23] Doping by Ce offered another effective way to improve the activity of $Ln_2O_2SO_4$ (Ln ≠ Ce). It causes structural distortion of tetrahedral SO_4 units, promoting the rates of oxygen release and storage,[24] while the co-presence of Ce^{3+}/Ce^{4+} ions on the surface of $Ln_2O_2SO_4$ further accelerated the redox of sulfur. The detailed X-ray structural study revealed that the oxygen release and storage behavior is accompanied by noticeable differences in S–O distances and O–S–O angles of the SO_4 units, as well as

Department of Biotechnology, Delft University of Technology, Julianalaan 136, 2628 BL Delft, the Netherlands. E-mail: k.djanashvili@tudelft.nl

†Electronic supplementary information (ESI) available: Experimental procedures, TGA profiles, TEM images, and EDS spectra of $Pr_2O_2SO_4$. See DOI: 10.1039/c6dt01667g

differences in the crystal structure of $Ln_2O_2^{2+}$ units.[22,25] In a very recent report, Lisi *et al.* demonstrated that Cu-doping can enhance the oxygen mobility in the $La_2O_2SO_4$ structure, leading to decreased reaction temperatures for both reduction and oxidation.[20]

The $Ln_2O_2SO_4$ materials for oxygen storage and release reported so far have been prepared by several methods, such as calcination of $Ln_2(SO_4)_3{\cdot}nH_2O$,[1,26] utilization of precursors of layered Ln-dodecyl sulfate mesophases,[23,27] or Ln-precipitation.[28,29] All these procedures lead to bulk materials with an irregular morphology. The correlation between the size and shape of the catalyst and the catalytic performance has been mentioned in the literature,[30–32] but the effects on oxygen storage/release performance have yet not been demonstrated. Herein we report on a remarkable enhancement of the oxygen storage/release capacity by (i) using nanosized $Pr_2O_2SO_4$ rather than bulk and (ii) by doping the $Pr_2O_2SO_4$ with Ni(II). $Pr_2O_2SO_4$ was selected, because among the lanthanides it can act as oxidation catalyst with high rates at relatively low temperatures (<600 °C).[1]

Recently, we have developed a facile method for the preparation of nanosized $Ln_2O_2SO_4$ (Ln = Gd and Ho) based on thermal decomposition of nanodroplets (NDs) formed by Ln-acetylacetonates (Ln(acac)$_3$) under emulsifying conditions.[33] The choice of the surfactant for the formation of NDs was found to determine the elemental composition of the nanoparticles (NPs) obtained after the calcination of the dried NDs. In the present study sodium dodecyl sulfate was selected as the surfactant. The thermogravimetric analysis (TGA) profile of the fluffy powders resulting from freeze drying of the obtained NDs, showed two major weight losses: dehydration and combustion of organic moieties below 300 °C (Fig. S1†). The formation of $Pr_2O_2SO_4$ takes place between 300–800 °C by the alternative stacking between SO_4^{2-} and $Pr_2O_2^{2+}$.[23,24] Above 800 °C a stabilized curve was observed, indicating the full formation of inorganic NPs after this temperature. Therefore, to obtain the solid NPs, the calcination was carried out at 800 °C for 1 h to give $Pr_2O_2SO_4$ NPs in 82% yield with respect to Pr(acac)$_3$.

Fig. 1 demonstrates the X-Ray Diffraction (XRD) patterns of the crystalline $Pr_2O_2SO_4$ as well as the oxysulfide Pr_2O_2S, which was obtained after reduction of the oxysulfate by H_2 (10%) in Ar. The XRD pattern reveals an orthorhombic structure of $Pr_2O_2SO_4$ with calculated lattice constants a = 4.240 Å, b = 4.138 Å, and c = 13.422 Å, which are in a good agreement with the reported values (PDF#41-0679). Additionally, the XRD pattern of Pr_2O_2S shows lattice dimensions of a = 3.574 Å, b = 3.974 Å and c = 6.798 Å, corresponding to a hexagonal cell (p3ml-164, PDF#65-3453). TEM images show that fairly spherical particles NPs were obtained with a diameter of 28 ± 5.1 (Fig. S2†).

Following the successful preparation of $Pr_2O_2SO_4$ NPs, their redox behavior was investigated (Fig. 2a and b). The dynamic reduction was evaluated by the temperature programmed reduction (TPR), which was carried out in a conventional flow system by heating the sample at 10 °C min^{-1} in a stream of 10% H_2 in Ar. As shown in Fig. 2a, the reduction started at about 700 °C and gave a peak in H_2-uptake at 790 °C, whereas the reaction was completed at around 800 °C. The asymmetric peak in the narrow temperature range indicated a very fast reduction. The oxysulfate was reduced into oxysulfide (Pr_2O_2S), as proven by its XRD pattern as shown in Fig. 1. The obtained oxysulfide was then subjected to temperature programmed re-oxidation (TPRO) in a stream of 20% O_2 in He (Fig. 2b). The oxygen consumption started at about 480 °C and exhibited a maximal peak at 580 °C. Above this temperature, the re-oxidation rate became slower and was not even completed until 900 °C. Based on the integration of TPR and TPRO profiles, the amount of consumed H_2 and O_2 was 3.97 and 1.34 mol^{-1} for $Pr_2O_2SO_4$ and Pr_2O_2S, respectively. The ratio of oxygen

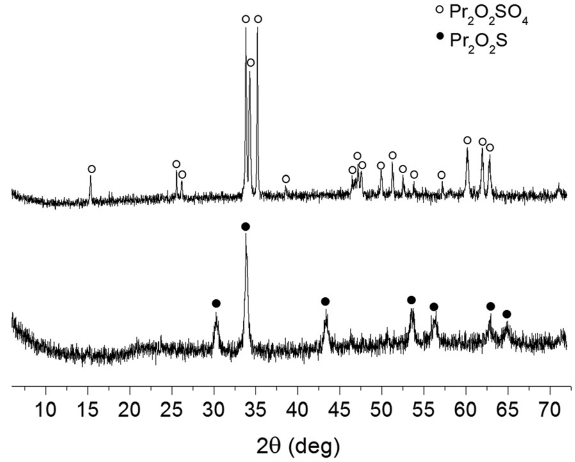

Fig. 1 Powder XRD patterns of nanoparticulate $Pr_2O_2SO_4$ obtained by miniemulsion method, and Pr_2O_2S, resulted from the subsequent reduction.

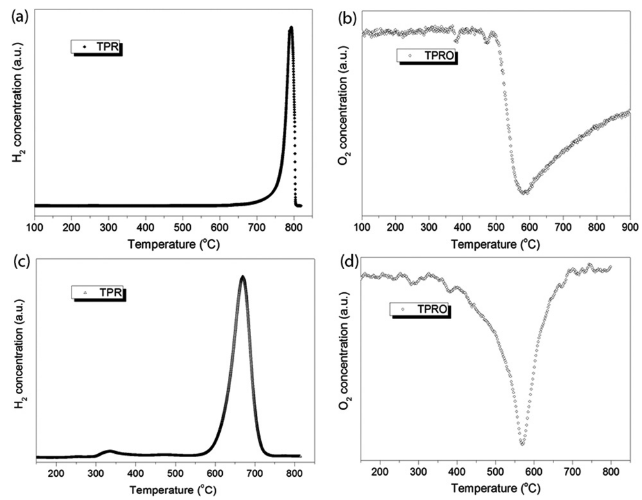

Fig. 2 Temperature programmed profiles of redox reactions catalyzed by nanoparticulate $Pr_2O_2SO_4$: on the left are TPR profiles of non-doped (a) and 1.9% Ni-doped (c) $Pr_2O_2SO_4$ in a flow of 10% H_2/Ar and on the right are TPRO profiles of non-doped (b) and 1.9% Ni-doped (d) $Pr_2O_2SO_4$ in a flow of 20% O_2/He. Heating rate 10 °C min^{-1}.

consumption per mol of Pr_2O_2S is somewhat below 2, which confirms that the re-oxidation was not finished under the conditions applied.

These results can be compared with those for the bulk material as reported in literature.[1] The nanosized $Pr_2O_2SO_4$ displays a fast reduction in TPR between 700 and 800 °C, and a low temperature for the maximum uptake of oxygen in TPRO (580 °C). In contrast, the catalytic performance of the previously reported bulk $Pr_2O_2SO_4$ was clearly less effective: the reduction took place above 900 °C and the maximum oxygen uptake was observed only at 700 °C.[1]

Aiming at further enhancement of the redox reactions, we next doped the $Pr_2O_2SO_4$ with Ni(II) as a cost-effective alternative for Pt or Pd for activation of both hydrogen and oxygen.[2,34] The $Pr_2O_2SO_4$ NPs described above were impregnated with an aqueous solution of $NiCl_2$ and then calcined at 450 °C for 90 min to give $Pr_2O_2SO_4$ doped with 1.9 wt% of Ni. The extent of Ni-doping was calculated from the Energy Dispersive Spectrum (EDS) of the prepared materials (Fig. S3†). The identical XRD-patterns (Fig. S4†) confirm the unchanged crystallinity of $Pr_2O_2SO_4$ NPs after doping with Ni, as it was already expected from the literature data.[35] Additionally, the calculations of the lattice space selected from the HRTEM images (Fig. S5†) resulted in 1.57, 0.72, 0.55, 0.45 and 0.36 nm, corresponding to the interplanar space of (001), (002), (100), (100), (310) and (202) crystallographic plane, which is a fair agreement with the interplanar space of the standard (PDF#41-0679).

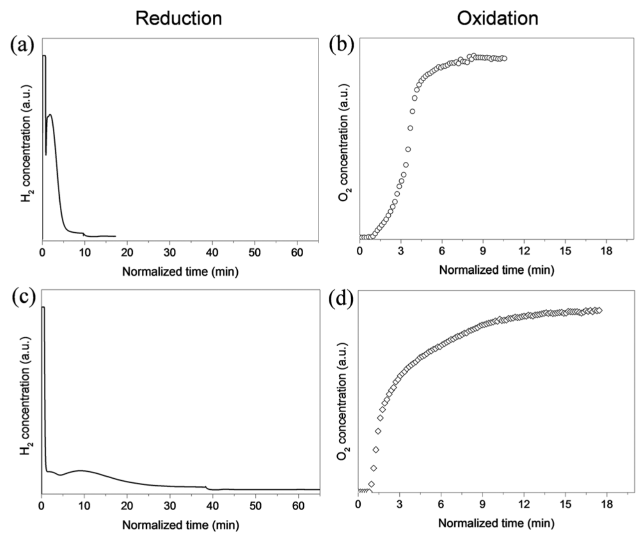

Fig. 3 Redox reactions of 1.9 wt% Ni-doped $Pr_2O_2SO_4$ at 700 °C (a, b) and 600 °C (c, d) under feed stream of 10% H_2/Ar and 5% O_2/He.

The TPR/TPRO profile of these Ni-doped NPs (Fig. 2c and d) appeared to release the oxygen in the temperature range 570–730 °C under consumption of 3.89 mol^{-1} of H_2. The oxygen uptake started at about 400 °C, reached a maximum at 580 °C, and was completed at about 700 °C with 1.93 mol^{-1} of the total O_2 uptake. The ratio H_2/O_2 uptake is 2, which is in perfect agreement with fully reversible redactions.

The rate of oxygen release and storage is another important property that characterizes the performance of the $Ln_2O_2SO_4$ as a storage material. To compare this property of the present nanosized $Pr_2O_2SO_4$ with those of the bulk material, we performed the redox reaction at both 700 and 600 °C, as shown in Fig. 3. Because this material has demonstrated perfect dynamic oxygen release and storage cycles, we only calculated the reaction rates based on the first cycle. For the 1.9 wt% Ni-doped $Pr_2O_2SO_4$ NPs, both reduction and re-oxidation reactions were completed within 10 min at 700 °C. The reaction rates calculated from the redox profiles are 0.51 mmol g^{-1} min^{-1} for the reduction, and 0.66 mmol g^{-1} min^{-1} for the re-oxidation. The rate of oxygen storage is more than 2 times higher than that of the best bulk $Pr_2O_2SO_4$ materials doped with 1 wt% Pd reported in the literature (see Table 1). At 600 °C, the storage rate of Ni-doped $Pr_2O_2SO_4$ is still faster than that of bulk material measured at 700 °C. The observed faster oxygen storage compared to release is in agreement with bulk materials, and is characteristic for the Pr-based systems. This is due to the coexistence of Pr^{3+} and Pr^{4+} ions on the particle surface as demonstrated by Machida and coworkers.[22,25]

These results show that the Ni-doped nanosized $Pr_2O_2SO_4$ system has an improved performance in terms of faster reaction rate at lower temperatures compared to bulk materials. This is likely to be due to the reduced size of the particles: the higher surface-to-volume ratio of smaller NPs leads to rapid gas diffusion and solid–gas reactions that facilitate oxygen storage and release.[23,26] Additionally, smaller size leads to an increased number of Pr^{3+} and Pr^{4+} species on the surface of NPs. As discussed above, the obtained $Pr_2O_2SO_4$ NPs exhibit orthorhombic structure with shortened a (4.240 Å) but extended c (13.422 Å) of lattice parameters, compared to those of the bulk material with a monoclinic structure (a = 14.047 Å, and c = 8.281 Å).[22] Stacking of $SO_4{}^{2-}$ and $Pr_2O_2{}^{2+}$ layers along the a-axis changes the crystal structure of $Pr_2O_2SO_4$ NPs by distortion of the SO_4 tetrahedral units in which each oxygen atom is coordinated to a Pr atom.[30] This is, therefore, probably

Table 1 Oxygen release and storage properties of $Pr_2O_2SO_4$ materials

Catalyst	Reaction temp./°C	O_2 release/ mmol g^{-1} min^{-1}	O_2 storage/ mmol g^{-1} min^{-1}	Ref.
Bulk $Pr_2O_2SO_4$ (1 wt% Pd-doping)	700	0.325	0.325	25
Bulk $Pr_2O_2SO_4$ (1 wt% Pd-doping)	600	0.07	N.A.	30
$Pr_2O_2SO_4$ NPs (1.9 wt% Ni-doping)	700	0.51	0.66	This work
$Pr_2O_2SO_4$ NPs (1.9 wt% Ni-doping)	600	0.13	0.36	This work

advantageous for the faster release of oxygen observed in the present study.

In summary, the nanoparticulate $Pr_2O_2SO_4$ showed a remarkable enhancement of oxygen storage/release reaction rates allowing operation with good performance at lower temperatures than comparable bulk Pr-oxysulfates. Further improvement was achieved by 1.9 wt% doping with Ni, due to increased oxygen mobility known to occur at the surface of the catalysts with available d-orbitals. The results of TPR/TPRO for the Ni-doped $Pr_2O_2SO_4$ show catalytic activity already at 600 °C, and 700 °C, and the rates for oxygen storage and release are respectively 2 and 4.6 times higher than these of the best bulk material reported up to now (1 wt% Pd-doped $Pr_2O_2SO_4$). The promoting effect of the presented system could be attributed to a collective effect of (i) higher surface-to-volume ratio of NPs, (ii) co-presence of Pr^{3+} and Pr^{4+} at the NP surface, (iii) distorted crystal structure leading to more reactive SO_4 units, and (iv) Ni-doping as a cost-effective alternative to much more expensive Pt and Pd. These effects result in an overall enhanced ability in storing and releasing oxygen.

Acknowledgements

This research was supported by China Scholarship Council (W. Z.) and the Netherlands Organization for Scientific Research (K. D., Veni grant-722.012.009). The authors thank Bart van der Linden (Catalysis Engineering, TU Delft) for the TPR/TPRO measurements.

Notes and references

1 M. Machida, K. Kawamura, K. Ito and K. Ikeue, *Chem. Mater.*, 2005, **17**, 1487–1492.
2 J. Wang, H. Chen, Z. Hu, M. Yao and Y. Li, *Catal. Rev.: Sci. Eng.*, 2015, **57**, 79–144.
3 T. Motohashi, T. Ueda, Y. Masubuchi, M. Takiguchi, T. Setoyama, K. Oshima and S. Kikkawa, *Chem. Mater.*, 2010, **22**, 3192–3196.
4 W. Yu, M. D. Porosoff and J. G. Chen, *Chem. Rev.*, 2012, **112**, 5780–5817, and references therein.
5 T. Osaki, K. Yamada, K. Watari and K. Tajiri, *React. Kinet., Mech. Catal.*, 2014, **114**, 561–570.
6 N. J. Lawrence, J. R. Brewer, L. Wang, T.-S. Wu, J. Wells-Kingsbury, M. M. Ihrig, G. Wang, Y.-L. Soo, W.-N. Mei and C. L. Cheung, *Nano Lett.*, 2011, **11**, 2666–2671.
7 B. Huang, R. Gillen and J. Robertson, *J. Phys. Chem. C*, 2014, **118**, 24248–24256.
8 A. Simson, K. Roark and R. Farrauto, *Appl. Catal., B*, 2014, **158–159**, 106–111.
9 N. Qiu, J. Zhang and Z. Wu, *Phys. Chem. Chem. Phys.*, 2014, **16**, 22659–22664.
10 Q. Dong, S. Yin, C. Guo, X. Wu, T. Kimura, T. Le, T. Sakanakura and T. Sato, *IOP Conf. Ser.: Mater. Sci. Eng.*, 2013, **47**, 012065.
11 J. Li, Z. Zhang, Z. Tian, X. Zhou, Z. Zheng, Y. Ma and Y. Qu, *J. Mater. Chem. A*, 2014, **2**, 16459–16466.
12 M. P. Yeste, J. C. Hernandez-Garrido, D. C. Arias, G. Blanco, J. M. Rodriguez-Izquierdo, J. M. Pintado, S. Bernal, J. A. Perez-Omil and J. J. Calvino, *J. Mater. Chem. A*, 2013, **1**, 4836–4844.
13 C. Sun and D. Xue, *Phys. Chem. Chem. Phys.*, 2013, **15**, 14414–14419.
14 H. Imagawa, A. Suda, K. Yamamura and S. Sun, *J. Phys. Chem. C*, 2011, **115**, 1740–1745.
15 J. Kašpar and P. Fornasiero, *J. Solid State Chem.*, 2003, **171**, 19–29.
16 N. S. Nasri, J. M. Jones, V. A. Dupont and A. Williams, *Energy Fuels*, 1998, **12**, 1130–1134.
17 L. S. Carvalho, C. L. Pieck, M. do Carmo Rangel, N. S. Fígoli and J. M. Parera, *Ind. Eng. Chem. Res.*, 2004, **43**, 1222–1226.
18 H. Tian and Q. Guo, *Ind. Eng. Chem. Res.*, 2009, **48**, 5624–5632.
19 Q. Song, R. Xiao, Z. Deng, H. Zhang, L. Shen, J. Xiao and M. Zhang, *Energy Convers. Manage.*, 2008, **49**, 3178–3187.
20 L. Lisi, G. Mancino and S. Cimino, *Int. J. Hydrogen Energy*, 2015, **40**, 2047–2054.
21 M. Machida, K. Kawamura and K. Ito, *Chem. Commun.*, 2004, 662–663.
22 M. Machida, T. Kawano, M. Eto, D. Zhang and K. Ikeue, *Chem. Mater.*, 2007, **19**, 954–960.
23 M. Machida, K. Kawamura, T. Kawano, D. Zhang and K. Ikeue, *J. Mater. Chem.*, 2006, **16**, 3084–3090.
24 D. Zhang, F. Yoshioka, K. Ikeue and M. Machida, *Chem. Mater.*, 2008, **20**, 6697–6703.
25 K. Ikeue, T. Kawano, M. Eto, D. Zhang and M. Machida, *J. Alloys Compd.*, 2008, **451**, 338–340.
26 X. Ye, J. E. Collins, Y. Kang, J. Chen, D. T. N. Chen, A. G. Yodh and C. B. Murray, *Proc. Natl. Acad. Sci. U. S. A.*, 2010, **107**, 22430–22435.
27 D.-J. Zhang, M. Eto, K. Ikeue and M. Machida, *J. Ceram. Soc. Jpn.*, 2007, **115**, 597–601.
28 W. Shen and S. Naito, *Adv. Mater. Res.*, 2014, **886**, 196–199.
29 Y. Liu, D. Tu, H. Zhu and X. Chen, *Chem. Soc. Rev.*, 2013, **42**, 6924–6958.
30 E. Aneggi, D. Wiater, C. de Leitenburg, J. Llorca and A. Trovarelli, *ACS Catal.*, 2014, **4**, 172–181.
31 C. Sun and D. Xue, *Phys. Chem. Chem. Phys.*, 2013, **15**, 14414–14419.
32 H. Imagawa, A. Suda, K. Yamamura and S. Sun, *J. Phys. Chem. C*, 2011, **155**, 1740–1745.
33 W. Zhang, J. Martinelli, F. Mayer, C. S. Bonnet, F. Szeremeta and K. Djanashvili, *RSC Adv.*, 2015, **5**, 69861–69869.
34 R. Ran, X. Wu, D. Weng and J. Fan, *J. Alloys Compd.*, 2013, **577**, 288–294.
35 K. Ikeue, M. Eto, D.-J. Zhang, T. Kawano and M. Machida, *J. Catal.*, 2007, **248**, 46–52.